PHYSICAL MODEL OF THE CHINESE YEHU FOR SOUND SYNTHESIS

Zhen Zheng, Champ C. Darabundit, and Gary Scavone

CAML, CIRMMT
Schulich School of Music, McGill University
Montreal, Canada
zhen.zheng@mail.mcgill.ca

ABSTRACT

The yehu is a Chinese bowed string instrument featuring a resonator carved from a coconut shell, a seashell-based bridge, and two silk strings. This paper proposes a physical model of the yehu and reports on simulations using a finite-difference scheme with measurement-based physical characterization. The proposed model consists of two stiff strings coupled at the bridge, a bow with elastic bow hairs, a stopping finger, and a modal model of the bridge. A non-iterative solver based on energy quadratization is used to model the finger–string contact force, while an iterative solver is used for elasto-plastic bow-string friction force. The bridge-body model is based on a modal characterization obtained from the measured bridge admittance. The measured radiation transfer function is represented as a bank of parallel second-order filters and is applied to the simulated bridge force to incorporate body radiation characteristics. Finally, computational performance tests are conducted, showing that the proposed model is capable of real-time computation.

1. INTRODUCTION

The yehu is a bowed string instrument with two fixed silk strings (typically tuned to F4 and C5) and the bow positioned between them, as shown in the left of Fig. 1. The instrument does not have a fingerboard. To vary the pitch of the instrument, the player uses their fingers to stop the strings directly. The two strings are close together and the performer typically stops both strings simultaneously. At the bridge, the strings press against a seashell bridge mounted on a wooden plate that is rigidly attached to the carved coconut resonator. The effective vibrating length of the yehu string extends from the restraining loop to the bridge. However, to capture the string-bridge coupling dynamics, the strings are modeled over an extended domain from the restraining loop to the stub, as shown in the right of Fig. 1. Although it is possible to excite both strings simultaneously, performers typically only bow one string at a time, and the yehu is generally treated as a monophonic instrument.

Bowed string instrument modeling requires an appropriate description of the friction between the bow and string. Static friction models describe the friction force as a function of relative velocity, such as the friction curve models in [1][2], while dynamic models include an elasto-plastic formulation [3] and a thermal friction model [4]. Both types have been extended to time-domain simulations, using digital waveguide (DWG) and finite-difference (FD) schemes [5][6][7]. More recent developments incorporate additional mechanisms, such as finite-width bow interaction and torsional string motion [8][9]. Beyond friction, the vibration of the string is shaped by its coupling with the bridge and instrument body. Several approaches have been proposed to model this interaction. A wave-propagation model can simulate coupling using both reflection and transmission filters [10], modal approaches introduce coupling via projection onto the modal basis, resulting in globally coupled modes [11]. Pitch variation in bowed-string instruments is achieved through finger–string contact. This interaction is commonly modeled as a collision [7][12], with parameters tuned to approximate the mechanical properties of the finger. Energy-conserving FD schemes based on iterative solvers have been proposed [13][14], while more recent non-iterative methods based on energy quadratization significantly improve computational efficiency [15][16].

This paper is structured as follows. Section 2 contains the

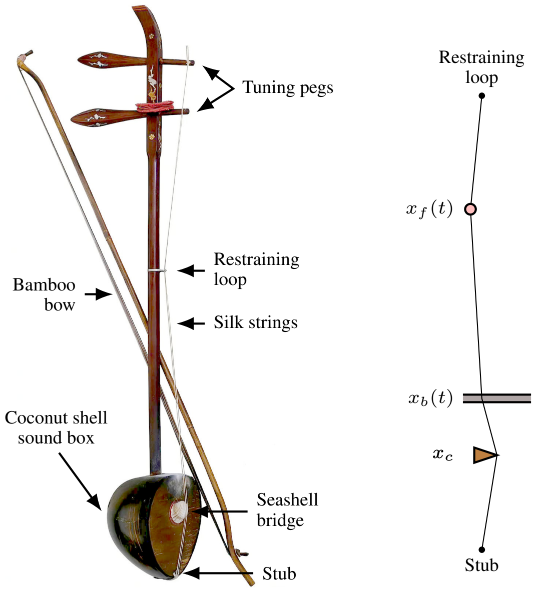

Figure 1: Left: A picture of the author's yehu with parts labeled. The bow hair passes between the two strings. Right: Side view of a simplified model of the yehu. The string is simply supported at the restraining loop and stub. The string is coupled to the bridge and body at x_c. The finger and bow interact with string at $x_f(t)$ and $x_b(t)$, respectively.

equations that describe the proposed system. An energy balanced FD scheme is presented in Section 3. Section 4 presents the physical characterization of the model by measurements, while Section 5 presents the simulation results. Section 6 concludes the paper.

2. MODEL DESCRIPTION

2.1. String equations

The proposed yehu model can be divided into three forces interacting with two stiff strings: the finger-string contact force f_f, bowed string friction force f_b and bridge coupling force f_c. In the following part, we annotate the inner string (F4) as string one and the outer string (C5) as string two with $i = 1, 2$, respectively. The partial differential equation governing the time evolution of the two strings' transversal displacement $u_i(x_i, t)$ can be written as:

$$\mathcal{L}_{s,i} u_i = -J_{b,i} f_{b,i} - J_{f,i} f_{f,i} + J_{c,i} f_{c,i}. \tag{1}$$

Here, $x_i \in \mathcal{D}_{L_i} = \{x_i \in \mathbb{R} \mid 0 \leq x_i \leq L_i\}$ and L_i is the string length. $f_{b,i}$, $f_{f,i}$ and $f_{c,i}$ are the friction force, finger contact force, and bridge coupling force, respectively, acting on each string. $J_{b,i}$, $J_{f,i}$, and $J_{c,i}$ are spatial distribution functions that map the forces from an interaction point to the string domain. $\mathcal{L}_{s,i}$ is the partial differential operator defined as:

$$\rho_i A_i \partial_t^2 - T_i \partial_{x,i}^2 + E_i I_i \partial_{x,i}^4 + 2\rho_i A_i \partial_t \left(\sigma_{0,i} - \sigma_{1,i} \partial_{x,i}^2\right), \tag{2}$$

in which ρ_i, A_i, T_i, E_i, and I_i denote mass density ($\mathrm{kg} \cdot \mathrm{m}^{-3}$), cross-sectional area (m^2), tension (N), Young's modulus (Pa), and area moment of inertia (m^4) for each string i, respectively. The parameters $\sigma_{0,i}$ (s^{-1}) and $\sigma_{1,i}$ (m^2/s) are loss coefficients accounting for frequency-independent and frequency-dependent losses. The boundaries of each string are simply supported:

$$u_i(0,t) = u_i(L,t) = 0,\ \partial_{x,i}^2 u_i(0,t) = \partial_{x,i}^2 u_i(L,t) = 0. \tag{3}$$

2.2. Finger-string contact

The contact force between the finger and the string, denoted by $f_{f,i}$, can be formulated using the Hunt-Crossley contact model [13]

$$f_{f,i} = \frac{d\Phi_i}{d\eta_i} + \frac{d\eta_i}{dt}\Theta_i, \tag{4}$$

where the contact potential, Φ_i, and the dissipation term, Θ_i, are defined as

$$\Phi_i = \frac{K_f [\eta_i]_+^{\alpha+1}}{\alpha+1}, \qquad \Theta_i = \beta K_f [\eta_i]_+^{\alpha}. \tag{5}$$

$\beta \geq 0$ is the finger damping coefficient, $K_f \geq 0$ is the finger stiffness parameter, $\alpha > 1$ is a nonlinear coefficient, and $[\eta_i]_+$ is the finger-string penetration, defined as:

$$\eta_i = \int_{\mathcal{D}_{L_i}} J_{f,i}(x_{f,i}, t)\, u_i(x_i, t)\, dx_i - U_f, \quad [\eta_i]_+ = \max\left(0, \eta_i\right). \tag{6}$$

$J_{f,i}(x_{f,i}, t)$ is the spatial distributed function of finger location at x_f and $U_f(t)$ is the position of the vertical finger at time t. In order to reduce the computation cost, a non-iterative solver based on energy quadratization is utilized. Defining the potential function Φ_i [16][15],

$$\Phi_i = \frac{\Psi_i^2}{2}, \tag{7}$$

and applying the chain rule to (7), (4) may be written as

$$f_{f,i} = \Psi_i g_i + \beta \Psi_i \frac{d\Psi_i}{dt}, \quad \frac{d\Psi_i}{dt} = g_i \frac{d\eta_i}{dt}, \quad g_i = \partial_\eta \Psi_i. \tag{8}$$

The finger motion is governed by

$$M_f \frac{d^2 U_f}{dt^2} = f_{f,1} + f_{f,2} + f_{\text{ext}}, \tag{9}$$

where M_f is the finger mass (kg), and $f_{\text{ext}}(t)$ is the external force (N) driving the finger.

2.3. String-bridge coupling

The bridge is modeled as a set of M mass-spring-damper (MSD) systems representing a modal expansion of the measured bridge admittance.

$$M_m \frac{d^2 q_m}{dt^2} + K_m q_m + R_m \frac{dq_m}{dt} = -f_{c,1} - f_{c,2}, \tag{10}$$

where q_m is the modal displacement (m), M_m is the modal mass (kg), K_m is the modal spring constant (N/m), and R_m is the modal damping term (kg/s), which are defined by

$$R_m = M_m \sigma_m \omega_m, \quad K_m = M_m \omega_m^2, \tag{11}$$

with σ_m the modal damping ratio, and ω_m the resonant frequency in rad/s of each mode. The strings are tightly coupled to the bridge and are assumed to exhibit negligible collision. Therefore, the displacement of the strings at the bridge position is assumed to be equal to the bridge displacement

$$\int_{\mathcal{D}_{L_i}} J_{c,i}(x_{c,i}, t)\, u_i(x_i, t)\, dx_i = \sum_{m=1}^{M} q_m(t). \tag{12}$$

2.4. Bow excitation

As the performance technique of yehu avoids bowing two strings simultaneously, the proposed model uses a signed bow force F_N to determine which string is bowed. In the following section, due to the large number of parameters involved, the bow–string interaction is presented for only one string. The friction force f_b is calculated using an elasto-plastic friction model which assumes that the friction between the bow and the string is the result of a large ensemble of microscopic elastic bristles, each contributing to the overall friction force [3]. Once the strain exceeds a breakaway threshold, the bristles lose adhesion, leading to sliding between the two surfaces. Denoting the average bristle deflection by z, the friction force can be described as [9]:

$$f_b = \epsilon_0 z + \epsilon_1 \frac{dz}{dt}, \tag{13}$$

where ϵ_0 is the bristle stiffness in N/m, ϵ_1 is the bristle damping in kg/s, and v_r is the relative velocity, defined as:

$$v_r = \frac{d}{dt}\left(\int_{\mathcal{D}_L} J_b(x,t) u(x,t)\right) dx + \frac{d}{dt}\zeta(t) - v_b(t), \tag{14}$$

with $\zeta(t)$ the bow hair displacement in meters relative to the rigid bow. The motion of bow hair can be described with bow hair mass M_f in kg, stiffness K_h in N/m, and damping R_h in kg/s:

$$M_h \frac{d^2\zeta}{dt^2} + K_h \zeta + R_h \frac{d\zeta}{dt} = -f_b. \tag{15}$$

The bristle velocity is related to the relative velocity v_r through

$$\frac{dz}{dt} = v_r\left[1 - \chi(v_r, z)\frac{z}{z_{ss}(v_r)}\right], \tag{16}$$

where z_{ss} is the steady-state function,

$$z_{ss}(v_r) = \text{sign}(v_r)\frac{F_N}{\epsilon_0}\left(\mu_C + (\mu_S - \mu_C)e^{-\left|\frac{v_r}{v_s}\right|^2}\right), \tag{17}$$

with Stribeck velocity, v_s, in m/s, static and dynamic friction coefficients, μ_S and μ_C, respectively, and normal force in N applied by the bow, F_N. The adhesion map, χ, is defined as

$$\chi(v_r, z) = \begin{cases} 0, & v_r z \le 0 \\ \chi_m, & v_r z > 0 \end{cases}, \tag{18}$$

where

$$\chi_m(z, v_r) = \begin{cases} 0, & |z| \le z_{ba} \\ \bar{\chi}_m(v_r, z), & z_{ba} < |z| < |z_{ss}(v_r)| \\ 1, & |z| \ge |z_{ss}(v_r)| \end{cases} \tag{19}$$

The breakaway displacement is $z_{ba} \le \xi\mu_C F_N/\epsilon_0$ with the free parameter $0 < \xi \le 1$. $\bar{\chi}_m(z, v_r)$ can be defined as

$$\bar{\chi}_m(z, v_r) = \frac{1}{2}\left[1 + \sin\left(\pi\frac{|z| - \frac{1}{2}(|z_{ss}(v_r)| + z_{ba})}{|z_{ss}(v_r)| - z_{ba}}\right)\right]. \tag{20}$$

2.5. Energy analysis

Taking the inner product of (1) with $\partial_t u_i$ over $\mathcal{D}_{L_i}$ for each string, multiplying equation (9) with $\partial_t U_f$, multiplying equation (10) with $\partial_t q_m$, summing the modes together, multiplying equation (15) with $\partial_t \zeta$, and using the relation in (14), the power-balance of the entire system is derived:

$$\frac{d\mathcal{H}}{dt} = \mathcal{P} - \mathcal{Q} + \mathcal{B}_s|_0^L \tag{21a}$$

$$\mathcal{H} = \mathcal{H}_s + \mathcal{H}_c + \mathcal{H}_f + \mathcal{H}_\zeta + \mathcal{H}_z \tag{21b}$$

Here, the energy stored in the string $\mathcal{H}_s$, finger $\mathcal{H}_f$, bridge $\mathcal{H}_c$, bow hair $\mathcal{H}_\zeta$ and bristle $\mathcal{H}_z$ are given by

$$\mathcal{H}_s = \sum_{i=1}^{2}\left[\frac{\rho_i A_i}{2}\|\partial_t u_i\|^2_{\mathcal{D}_{L_i}} + \frac{T_i}{2}\|\partial_x u_i\|^2_{\mathcal{D}_{L_i}} + \frac{E_i I_i}{2}\|\partial_{xx} u_i\|^2_{\mathcal{D}_{L_i}}\right], \tag{22a}$$

$$\mathcal{H}_f = \frac{M_f}{2}\left(\frac{dU}{dt}\right)^2 + \sum_{i=1}^{2}\frac{1}{2}\Psi_i^2, \tag{22b}$$

$$\mathcal{H}_c = \sum_{m=1}^{M}\left[\frac{M_m}{2}\left(\frac{dq_m}{dt}\right)^2 + \frac{K_m}{2}q_m^2\right], \tag{22c}$$

$$\mathcal{H}_\zeta = \sum_{i=1}^{2}\left[\frac{M_f}{2}\left(\frac{d\zeta_i}{dt}\right)^2 + \frac{K_h}{2}\zeta_i^2\right],\ \mathcal{H}_z = \sum_{i=1}^{2}\frac{\epsilon_0}{2}z_i^2. \tag{22d}$$

The power supplied to the system, $\mathcal{P}$ is

$$\mathcal{P} = f_{\text{ext}}\frac{dU}{dt} + f_{b,1}v_B + f_{b,2}v_B. \tag{23}$$

Total power dissipation related to the strings $\mathcal{Q}_s$, finger $\mathcal{Q}_f$, bridge $\mathcal{Q}_c$, bow hair $\mathcal{Q}_\zeta$, and bristles $\mathcal{Q}_z$ are given by

$$\mathcal{Q}_s = \sum_{i=1}^{2} 2\rho_i A_i\left(\sigma_{0,i}\|\partial_t u_i\|^2_{D_{L_i}} + \sigma_{1,i}\|\partial_{tx} u_i\|^2_{D_{L_i}}\right), \tag{24a}$$

$$\mathcal{Q}_f = \sum_{i=1}^{2}\beta g_i \Psi_i\left(\frac{d\eta_i}{dt}\right)^2, \quad \mathcal{Q}_c = \sum_{m=1}^{M} R_m\left(\frac{dq_m}{dt}\right)^2 \tag{24b}$$

$$\mathcal{Q}_\zeta = \sum_{i=1}^{2} R_h\left(\frac{d\zeta_i}{dt}\right)^2, \tag{24c}$$

$$\mathcal{Q}_z = \sum_{i=1}^{2}\left[\epsilon_1 v_{r,i}^2 - \chi(z_i, v_{r,i})\frac{z_i v_{r,i}}{z_{ss,i}}(\epsilon_0 z_i - \epsilon_1 v_{r,i})\right], \tag{24d}$$

$$\mathcal{Q} = \mathcal{Q}_s + \mathcal{Q}_f + \mathcal{Q}_c + \mathcal{Q}_z + \mathcal{Q}_\zeta. \tag{24e}$$

Under simply supported boundary conditions, the boundary term $\mathcal{B}_s$ vanishes. Note that $\mathcal{H}$, $\mathcal{Q}_s$, $\mathcal{Q}_f$, $\mathcal{Q}_c$ and $\mathcal{Q}_\zeta$ are all non-negative, and $\mathcal{Q}_z$ is non-negative whenever $\chi \ne 1$. But for $\chi = 1$, $\mathcal{Q}_z$ can become negative, which violates passivity and it is not physical. To solve this problem, [9] proposed a velocity-dependent bristle damping $\epsilon_1(v_r)$, that guarantees passivity

$$\epsilon_1(v_r) = \frac{\mu_C F_N}{\sqrt{v_r^2 + \gamma^2}}, \qquad \gamma = \frac{\mu_C F_N}{\bar{\epsilon}_1} \tag{25}$$

where $0 \le \epsilon_1(v_r) \le \bar{\epsilon}_1$ and $\bar{\epsilon}_1$ is a constant model parameter. With this refined definition, the term $\mathcal{Q}_z$ becomes non-negative, and the system is energy-stable. Proof of the non-negativity of $\mathcal{Q}_z$ can be found in [9].

3. NUMERICAL SCHEME

3.1. Grid function and difference operators

A finite difference scheme is applied to numerically solve the continuous domain equations. String displacement $u_i(x,t)$ is approximated by the grid function $u^n_{l,i}$, where n is the time index, and $l \in [0, ..., N_i]$ is the grid index. $\mathbf{u}^n_i \in \mathbb{R}^{(N_i-1)\times 1}$ is the vector representation of $u^n_{l,i}$ under fixed end condition. e_{t+} and e_{t-} denote forward and backward time shifts, respectively. A set of time difference operations may be defined as

$$\begin{aligned}
&\delta_{t+} = \frac{e_{t+} - 1}{k},\ \delta_{t-} = \frac{1 - e_{t-}}{k},\ \delta_{t\cdot} = \frac{e_{t+} - e_{t-}}{2k},\\
&\mu_{t+} = \frac{e_{t+} + 1}{2},\ \mu_{t-} = \frac{1 + e_{t-}}{2},\ \mu_{t\cdot} = \frac{e_{t+} + e_{t-}}{2},\\
&\delta_{t\circ} = \frac{e_{t+\frac{1}{2}} - e_{t-\frac{1}{2}}}{k}, \mu_{t\circ} = \frac{e_{t+\frac{1}{2}} + e_{t-\frac{1}{2}}}{2},\\
&\delta_{tt} = \frac{e_{t+} - 2 + e_{t-}}{k^2},\ \mu_{tt} = \frac{e_{t+} + 2 + e_{t-}}{4},
\end{aligned} \tag{26}$$

where k is the temporal sampling interval. A set of spatial difference matrices may be defined as

$$\mathbf{D}_i^- = \frac{1}{h_i}\begin{bmatrix} 1 & & 0 \\ -1 & \ddots & \\ & \ddots & 1 \\ 0 & & -1 \end{bmatrix} \in \mathbb{R}^{N_i\times(N_i-1)}, \tag{27}$$

$$\mathbf{D}_i^+ = -(\mathbf{D}_i^-)^T,\ \mathbf{D}_{2,i} = \mathbf{D}_i^+\mathbf{D}_i^-,\ \mathbf{D}_{4,i} = \mathbf{D}_i^2\mathbf{D}_i^2,$$

where h_i is the spatial sampling interval for each respective string. The continuous distribution functions $J(x,t)$ are discretized as polynomial spreading operators resulting in column vectors, $\mathbf{J}^n \in \mathbb{R}^{(N_i-1)\times 1}$ [17, Sec. 5.2.4]. The corresponding interpolation operators are $\mathbf{I}^n \in \mathbb{R}^{1\times(N_i-1)}$ defined as

$$\mathbf{I}^n = h\left(\mathbf{J}^n\right)^T. \tag{28}$$

The spatial inner product of two 1D grid functions, u_l^n and v_l^n over the domain $l \in d_N = [0,\dots,N]$ can be written as

$$\langle u_l^n, v_l^n\rangle = \sum_{l\in d_N} h u_l^n v_l^n. \tag{29}$$

The domains $d_{\underline{N}}$ and $d_{\overline{\underline{N}}}$ are partial domains omitting the left ($l=0$) boundary and both ($l=0$ and $l=N$) boundaries, respectively.

3.2. String operator discretization

The discretized form of the string displacement in (1) is

$$\mathbf{L}_{s,i}\mathbf{u}_i^n = -\mathbf{J}_{f,i}f_{f,i}^n - \mathbf{J}_{b,i}f_{b,i}^n + \mathbf{J}_{c,i}f_{c,i}^n, \tag{30}$$

where $\mathbf{u}_i$ is the vector containing the discrete string displacements. The spreading operators $\mathbf{J}_{f,i}, \mathbf{J}_{b,i}, \mathbf{J}_{c,i}$ are cubic, linear, and point operators [17, Sec. 5.2.4], respectively with the correct dimensions. The string operator (2) is discretized as

$$\begin{aligned}\mathbf{L}_{s,i} = {}& \rho_i A_i\delta_{tt} - T_i\mathbf{D}_{2,i} + E_iI_i\mathbf{D}_{4,i}\\ &+ 2\rho_iA_i\left(\sigma_{0,i}\delta_{t\cdot} - \sigma_{1,i}\delta_{t-}\mathbf{D}_{2,i}\right).\end{aligned} \tag{31}$$

The general update form for a single string is found by rearranging the discretized string operator,

$$A_{s,i}\mathbf{u}_i^{n+1} = \mathbf{B}_{s,i}\mathbf{u}_i^n + \mathbf{C}_{s,i}\mathbf{u}_i^{n-1} + \mathbf{J}_{s,i}\mathbf{f}_i^n, \tag{32}$$

where $A_{s,i} = \frac{\rho_iA_i}{k^2} + \frac{\rho_iA_i\sigma_{0,i}}{k}$, $\mathbf{B}_{s,i} = \frac{2\rho_iA_i}{k^2}\mathbf{1} + (T_i + \frac{2\rho_iA_i\sigma_{1,i}}{k})\mathbf{D}_{2,i} - E_iI_i\mathbf{D}_{4,i}$, $\mathbf{C}_{s,i} = (-\frac{\rho_iA_i}{k^2} + \frac{\rho_iA_i\sigma_{0,i}}{k})\mathbf{1} - \frac{2\rho_iA_i\sigma_{1,i}}{k}\mathbf{D}_{2,i}$. $\mathbf{f}_i^n = [-f_{f,i}^n, -f_{b,i}^n, f_{c,i}^n]^T \in \mathbb{R}^{3\times 1}$ is the vector of forces applied to the string i, and $\mathbf{J}_{s,i} = [\mathbf{J}_{c,i}^n, \mathbf{J}_{b,i}^n, \mathbf{J}_{f,i}^n] \in \mathbb{R}^{(N_i-1)\times 3}$. $\mathbf{1}$ denotes the identity matrix in $\mathbb{R}^{(N_i-1)\times(N_i-1)}$.

3.3. Finger-string contact based on energy quadratization

The finger contact force in (8) is discretized as,

$$\begin{aligned}f_{f,i}^n &= \left(\mu_{t+}\Psi_i^{n-\frac{1}{2}}\right)g_i^n + \beta\left(\delta_{t+}\Psi_i^{n-\frac{1}{2}}\right)\Psi_i^{n-\frac{1}{2}},\\ \delta_{t+}\Psi_i^{n-\frac{1}{2}} &= g_i^n\delta_{t\cdot}\eta_i^n,\\ g_i^n &= \theta_i\hat{g}_i^n = \theta_i\sqrt{\frac{1}{2}K_f(\alpha+1)[\eta_i^n]_+^{\alpha-1}}.\end{aligned} \tag{33}$$

To impose the constraint $\mu_{t+}\Psi_i^{n-\frac{1}{2}} \geq 0$, a scalar correction factor θ_i is introduced [12]. Let $\mathcal{V}_i = 4\Psi_i^{n-\frac{1}{2}} + \hat{g}_i^n(\eta_i^* - \eta_i^{n-1})$, and $\mathcal{R}_i^m = \hat{g}_i^m(\eta_i^* - \eta_i^{n-1}), m \in \{n, n-1\}$. Then θ_i is defined as

$$\theta_i = \begin{cases} -\dfrac{4\psi^{n-\frac{1}{2}}}{\mathcal{R}_i^n}, & \text{if } \mathcal{V}_i < 0 \,\&\, \mathcal{R}_i^n \neq 0,\\ -\dfrac{4\psi^{n-\frac{1}{2}}}{\mathcal{R}_i^{n-1}}, & \text{if } \mathcal{V}_i < 0 \,\&\, \mathcal{R}_i^n = 0 \,\&\, \mathcal{R}_i^{n-1} \neq 0,\\ 1, & \text{otherwise.}\end{cases} \tag{34}$$

Here, $\eta_i^* = \mathbf{I}_{f,i}\mathbf{u}_i^* - U_f^*$. $\mathbf{u}_1^*$, $\mathbf{u}_2^*$, and U_f^* denote the state updates (see (58)) for string one, string two, and the finger, respectively, in the absence of finger–string contact forces. By using the operator identity, $\mu_{t+} = \frac{k}{2}\delta_{t-} + 1$, and the discretization of (6), $\eta_i^n = \mathbf{I}_{f,i}\mathbf{u}_i - U^n$, $f_{f,i}^n$ can be rewritten as

$$f_{f,i}^n = \mathcal{A}_{f,i}\mathbf{I}_{f,i}\mathbf{u}_i^{n+1} - \mathcal{A}_{f,i}U^{n+1} + \mathcal{C}_{f,i}, \tag{35}$$

where $\mathcal{A}_{f,i} = \frac{g_i^{n2}}{4} + \frac{\beta g_i^n}{2k}\Psi_i^{n-\frac{1}{2}}$, $\mathcal{C}_{f,i} = -\frac{g_i^{n2}}{4}\eta_i^{n-1} + g_i^n\Psi_i^{n-\frac{1}{2}} - \frac{\beta g_i^n}{2k}\eta_i^{n-1}\Psi_i^{n-\frac{1}{2}}$. The finger displacement in (9) is discretized as,

$$M_f\delta_{tt}U_f^n = f_{f,1}^n + f_{f,2}^n + f_{\text{ext}}^n. \tag{36}$$

By substituting (35) into (30) and (36), the update can be written as

$$\begin{bmatrix}\mathbf{S}_1 & \mathbf{0} & \mathbf{S}_3\\ \mathbf{0} & \mathbf{S}_2 & \mathbf{S}_4\\ \mathbf{S}_5 & \mathbf{S}_6 & S_7\end{bmatrix}\begin{bmatrix}\mathbf{u}_1^{n+1}\\ \mathbf{u}_2^{n+1}\\ U_f^{n+1}\end{bmatrix} = \begin{bmatrix}\mathbf{b}_1 - \mathbf{J}_{f,1}\mathcal{C}_{f,1}\\ \mathbf{b}_2 - \mathbf{J}_{f,2}\mathcal{C}_{f,2}\\ b_3 + \mathcal{C}_{f,1} + \mathcal{C}_{f,2}\end{bmatrix}, \tag{37}$$

where $\mathbf{S}_i = (\frac{\rho_iA_i}{k^2} + \frac{\rho_iA_i\sigma_{0,i}}{k})\mathbf{1} + \mathbf{J}_{f,i}\mathbf{I}_{f,i}\mathcal{A}_{f,i}$, $\mathbf{S}_{i+2} = -\mathcal{A}_{f,i}\mathbf{J}_{f,i}$, $\mathbf{S}_{i+4} = -\mathcal{A}_{f,i}\mathbf{I}_{f,i}$, $S_7 = \frac{M_f}{k^2} + \mathcal{A}_{f,i}$, $\mathbf{b}_i = \mathbf{B}_{s,i}\mathbf{u}_i^n + \mathbf{C}_{s,i}\mathbf{u}_i^{n-1} - \mathbf{J}_{b,i}f_{b,i}^n + \mathbf{J}_{c,i}f_{c,i}^n$, and $b_3 = \frac{2M}{k^2}U_f^n - \frac{M}{k^2}U_f^{n-1} + f_{\text{ext}}^n$. To solve (37), the update can be performed blockwise, where each block takes the form of a diagonal matrix with a rank-one perturbation. Such matrices are invertible and admit an efficient inversion using the Sherman–Morrison formula [18]:

$$(\mathbf{A} + \boldsymbol{\alpha}\boldsymbol{\beta}^\top)^{-1} = \mathbf{A}^{-1} - \frac{\mathbf{A}^{-1}\boldsymbol{\alpha}\boldsymbol{\beta}^\top\mathbf{A}^{-1}}{1 + \boldsymbol{\beta}^\top\mathbf{A}^{-1}\boldsymbol{\alpha}}. \tag{38}$$

Here, $\mathbf{r}_1$, $\mathbf{r}_2$, and r_3 denote the first, second, and third block components of the right-hand side vector in (37), respectively. Consequently, $\mathbf{u}_1^{n+1}$ and $\mathbf{u}_2^{n+1}$ can be expressed as

$$\begin{aligned}\mathbf{u}_1^{n+1} &= \mathbf{S}_1^{-1}\mathbf{r}_1 - \mathbf{S}_1^{-1}\mathbf{S}_3U_f^{n+1},\\ \mathbf{u}_2^{n+1} &= \mathbf{S}_2^{-1}\mathbf{r}_2 - \mathbf{S}_2^{-1}\mathbf{S}_4U_f^{n+1}.\end{aligned} \tag{39}$$

Substituting (39) into the third block row yields

$$\left(S_7 - \mathbf{S}_5\mathbf{S}_1^{-1}\mathbf{S}_3 - \mathbf{S}_6\mathbf{S}_2^{-1}\mathbf{S}_4\right)U_f^{n+1} = r_3 - \mathbf{S}_5\mathbf{S}_1^{-1}\mathbf{r}_1 - \mathbf{S}_6\mathbf{S}_2^{-1}\mathbf{r}_2. \tag{40}$$

U_f^{n+1} can then be obtained by solving (40), after which $\mathbf{u}_1^{n+1}$ and $\mathbf{u}_2^{n+1}$ are updated using (39). Efficient inversion significantly accelerates the computation, making real-time implementation of the system feasible.

3.4. String-bridge coupling

The modal bridge system (10) is discretized as,

$$\hat{\mathbf{M}}_m\delta_{tt}\mathbf{q}^n + \hat{\mathbf{K}}_m\mu_{tt}\mathbf{q}^n + \hat{\mathbf{R}}_m^n\delta_{t\cdot}\mathbf{q}^n = -\mathbf{f}_{c,1}^n - \mathbf{f}_{c,2}^n, \tag{41}$$

where $\mathbf{f}_{c,1}^n$ and $\mathbf{f}_{c,2}^n$ are $M\times 1$ vectors with components containing corresponding scalar values $f_{c,1}^n$ and $f_{c,2}^n$. $\hat{\mathbf{M}}_m$, $\hat{\mathbf{K}}_m$, and $\hat{\mathbf{R}}_m$ denote the diagonal matrices constructed from the $M\times 1$ vectors $\mathbf{M}_m$, $\mathbf{K}_m$, and $\mathbf{R}_m$, respectively. Rearranging the equation, the update form for the bridge displacement is

$$\sum_{m=1}^{M} q_m^{n+1} = \mathbf{A}_q^T\mathbf{q}^n + \mathbf{B}_q^T\mathbf{q}^{n-1} - \mathbf{C}_q^T\left(\mathbf{f}_{c,1}^n + \mathbf{f}_{c,2}^n\right), \tag{42}$$

where $\mathbf{A}_q = \text{diag}(\mathbf{\Lambda})^{-1}\left(8\mathbf{M}_m - 2k^2\mathbf{K}_m\right)$, $\mathbf{B}_q = \text{diag}(\mathbf{\Lambda})^{-1}\left(-4\mathbf{M}_m - k^2\mathbf{K}_m + 2k\mathbf{R}_m\right)$, $\mathbf{C}_q = (\mathbf{\Lambda})^{-1}k^2$, $\mathbf{\Lambda} = 4\mathbf{M}_m + k^2\mathbf{K}_m + 2k\mathbf{R}_m$. Multiplying (32) by $\mathbf{I}^n_{c,i}$ and $A^{-1}_{s,i}$ yields:

$$\mathbf{I}^n_{c,i}\mathbf{u}^{n+1}_i = \mathbf{I}^n_{c,i}(A^{-1}_{s,i}\mathbf{B}_{s,i}\mathbf{u}^n_i + A^{-1}_{s,i}\mathbf{C}_{s,i}\mathbf{u}^{n-1}_i + A^{-1}_{s,i}\mathbf{J}^n_{c,i}f^n_{c,i}), \tag{43}$$

and the rigid coupling between the bridge and two strings is found by

$$u^{n+1}_{bri} = \sum_{m=1}^{M} q^{n+1}_m = \mathbf{I}^n_{c,1}\mathbf{u}^{n+1}_1 = \mathbf{I}^n_{c,2}\mathbf{u}^{n+1}_2. \tag{44}$$

Substituting (41) and (43) into (44), the coupling forces for string one and two, $f^n_{c,1}$, $f^n_{c,2}$, at time step n can be computed from,

$$\begin{bmatrix} S_{c_1} & \mathbf{o}^{\mathbf{T}}\mathbf{C}_q \\ \mathbf{o}^{\mathbf{T}}\mathbf{C}_q & S_{c_2} \end{bmatrix} \begin{bmatrix} f^n_{c,1} \\ f^n_{c,2} \end{bmatrix} = \begin{bmatrix} c_1 \\ c_2 \end{bmatrix}, \tag{45}$$

where $S_{c_i} = \mathbf{o}^{\mathbf{T}}\mathbf{C}_q + A^{-1}_{s,i}\mathbf{I}^n_{c,i}\mathbf{J}^n_{c,i}$, and $c_i = \mathbf{A}^{\mathbf{T}}_q\mathbf{q}^n + \mathbf{B}^{\mathbf{T}}_q\mathbf{q}^{n-1} - \mathbf{I}^n_{c,i}\left(A^{-1}_{s,i}\mathbf{B}_{s,i}\mathbf{u}^n_i + A^{-1}_{s,i}\mathbf{C}_{s,i}\mathbf{u}^{n-1}_i\right)$. $\mathbf{o} \in \mathbb{R}^{M\times 1}$ denotes the all-ones vector of size M.

3.5. Bow excitation

The bow-string interaction is numerically solved using a second-order discretization scheme on interleaved grids [9]. The discrete friction force f^n_b is formulated based on the elasto-plastic model as

$$f^n_b = \epsilon_0(\mu_{t\circ}z^n) + \epsilon_1(v^n_r)r^n, \tag{46}$$

where $r^n = \delta_{t\circ}z^n$ is the discrete bristle velocity. The bow hair displacement ζ is discretized using (15)

$$M_h\delta_{tt}\zeta^n + R_h\delta_{t\cdot}\zeta^n + K_h\mu_{tt}\zeta^n = -f^n_b. \tag{47}$$

The relative velocity can be discretized as

$$v^n_r = \mathbf{I}^n_b\delta_{t\cdot}\mathbf{u}^n + \delta_{t\cdot}\zeta^n - v^n_b. \tag{48}$$

Using the operator identity, $\delta_{tt} = \frac{2}{k}(\delta_{t\cdot} - \delta_{t-})$, (48) can be written

$$s^n - \mathcal{I}_J f^n_b - v^n_r - v^n_b = 0, \tag{49}$$

where

$$\begin{aligned} s^n &= \mathbf{I}^n_b(\mathbf{A}_b\mathbf{u}^n + \mathbf{B}_b\delta_{t-}\mathbf{u}^n) + \mathcal{A}_h\zeta^n + \mathcal{B}_h\delta_{t-}\zeta^n, \\ \mathcal{I}_J &= \frac{\mathbf{I}^n_b\mathbf{J}^n_b}{\rho A(\frac{2}{k} + 2\sigma_0)} + \frac{1}{(\frac{2M_h}{k} + \frac{kK_h}{2} + R_h)}. \end{aligned} \tag{50}$$

Here, $\mathbf{A}_b = T\mathbf{D}_2 - EI\mathbf{D}_4$, $\mathbf{B}_b = 2\rho A\sigma_1\mathbf{D}_2 + \frac{2\rho A}{k}\mathbf{1}$, $\mathcal{A}_h = -K/(\frac{2M_h}{k} + \frac{kK_h}{2} + R_h)$, and $\mathcal{B}_h = (\frac{2M}{k} + \frac{Kk}{2})/(\frac{2M_h}{k} + \frac{kK_h}{2} + R_h)$. Since f^n_b and r^n are nonlinearly dependent on the relative velocity, v^n_r, and the average bristle deflection, $\mu_{t\circ}z^n$, an iterative Newton-Raphson solver is applied. Defining the vector of unknowns as,

$$\mathbf{x} = [v^n_r,\ \mu_{t\circ}z^n]^{\mathbf{T}}, \tag{51}$$

substituting (46) and (50) into equation (49), and using the operator identity, $\delta_{t\circ} = \frac{2}{k}(\mu_{t\circ} - e_{t-\frac{1}{2}})$, the residual system $\mathbf{R}(\mathbf{x}) = 0$ is constructed

$$\mathbf{R}(\mathbf{x}) = \begin{bmatrix} s^n - \mathcal{I}_J f^n_b(v^n_r, \mu_{t\circ}z^n) - v^n_r - v^n_b \\ r^n(v^n_r, \mu_{t\circ}z^n) - \frac{2}{k}(\mu_{t\circ}z^n - z^{n-1/2}) \end{bmatrix} = \mathbf{0}. \tag{52}$$

The Jacobian matrix $\mathbf{J}_R = \partial\mathbf{R}/\partial\mathbf{x}$ is computed at each iteration $\mathcal{I}$:

$$\mathbf{J}_R = \begin{bmatrix} 1 + \mathcal{I}_J\frac{\partial f^n_b}{\partial v^n_r} & \mathcal{I}_J\frac{\partial f^n_b}{\partial(\mu_{t\circ}z^n)} \\ \frac{\partial r^n}{\partial v^n_r} & \frac{\partial r^n}{\partial(\mu_{t\circ}z^n)} - \frac{2}{k} \end{bmatrix}. \tag{53}$$

The update rule is $\mathbf{x}^{(\mathcal{I}+1)} = \mathbf{x}^{(\mathcal{I})} - \mathbf{J}^{-1}_R\mathbf{R}(\mathbf{x}^{(\mathcal{I})})$. Upon convergence, the next half-step bristle state is updated via $z^{n+1/2} = 2\mu_{t\circ}z^n - z^{n-1/2}$, the bristle velocity r^n is updated via $r^n = \frac{1}{k}(z^{n+1/2} - z^{n-1/2})$ and system variables, u^{n+1}, ζ^{n+1} are updated using the resulting friction force.

3.6. Discrete energy analysis

The energy balance for the proposed system is derived by taking the inner product of the governing equations with their respective time derivatives. By applying the summation-by-parts [17, Sec. 5.2.10] and accounting for boundary conditions, the discrete rate of change of the total system energy is expressed as,

$$\delta_{t-}\mathfrak{h}^{n+\frac{1}{2}} = \mathfrak{p}^n - \mathfrak{q}^n + \mathfrak{b}^n, \tag{54}$$

where the boundary term $\mathfrak{b}^n$ is equal to zero under simply supported conditions and the discrete stored energy $\mathfrak{h}^{n+\frac{1}{2}}$ is defined as the sum of the following components:

$$\mathfrak{h}^{n+\frac{1}{2}}_s = \sum_{i=1}^{2}\Bigg[\frac{\rho_i A_i}{2}\|\delta_{t+}\mathbf{u}^n_i\|^2_{d_{N_i}} + \frac{T_i}{2}\langle\delta_{x+}\mathbf{u}^n_i\delta_{x+}\mathbf{u}^{n+1}_i\rangle_{d_{\underline{N_i}}}, \tag{55a}$$

$$+\frac{E_iI_i}{2}\langle\delta_{xx}\mathbf{u}^n_i, \delta_{xx}\mathbf{u}^{n+1}_i\rangle_{d\underline{\overline{N_i}}} - \frac{\sigma_{1,i}k\rho_iA_i}{2}\|\delta_{t+}\delta_{x+}\mathbf{u}^n_i\|^2_{d_{\underline{N_i}}}\Bigg],$$

$$\mathfrak{h}^{n+\frac{1}{2}}_f = \frac{M_h}{2}(\delta_{t+}U^n)^2 + \sum_{i=1}^{2}\frac{(\Psi^{n+\frac{1}{2}}_i)^2}{2}, \tag{55b}$$

$$\mathfrak{h}^{n+\frac{1}{2}}_c = \sum_{m=1}^{M}\left[\frac{M_m}{2}(\delta_{t+}q^n_m)^2 + \frac{K_m}{2}(\mu_{t+}q^n_m)^2\right], \tag{55c}$$

$$\mathfrak{h}^{n+\frac{1}{2}}_\zeta = \sum_{i=1}^{2}\left[\frac{M_f}{2}(\delta_{t+}\zeta^n_i)^2 + \frac{K_h}{2}(\mu_{t+}\zeta^n_i)^2\right], \tag{55d}$$

$$\mathfrak{h}^{n+\frac{1}{2}}_z = \frac{\epsilon_0}{2}(z^{n+\frac{1}{2}}_1)^2 + \frac{\epsilon_0}{2}(z^{n+\frac{1}{2}}_2)^2. \tag{55e}$$

The power $\mathfrak{p}^n$, dissipation $\mathfrak{q}^n$ are defined on the time step n:

$$\mathfrak{p}^n = f^n_{\text{ext}}\delta_{t\cdot}U^n + (f^n_{b,1} + f^n_{b,2})v_B, \tag{56a}$$

$$\mathfrak{q}^n_s = \sum_{i=1}^{2}2\rho_iA_i\left(\sigma_{0,i}\|\delta_{t\cdot}\mathbf{u}^n_i\|^2_{d_{N_i}} + \sigma_{1,i}\|\delta_{t\cdot}\delta_{x+}\mathbf{u}^n_1\|^2_{d_{\underline{N_i}}}\right), \tag{56b}$$

$$\mathfrak{q}^n_f = \sum_{i=1}^{2}\beta g^n_i\Psi^{n-\frac{1}{2}}_i(\delta_{t\cdot}\eta^n_i)^2,\ \mathfrak{q}^n_c = \sum_{m=1}^{M}R_m(\delta_{t\cdot}q^n_m)^2, \tag{56c}$$

$$\mathfrak{q}^n_\zeta = \sum_{i=1}^{2}R_h(\delta_{t\cdot}\zeta^n_i)^2, \tag{56d}$$

$$\mathfrak{q}^n_z = \sum_{i=1}^{2}f^n_{b,i}v^n_{r,i} - \epsilon_0\mu_{t\circ}z^n_i\delta_{t\circ}z^n_i. \tag{56e}$$

For a given time step k, the term $\mathfrak{h}_s$ is non-negative under the condition $h_i \geq h_{\text{min},i}$[14], where

$$h^2_{\text{min},i} = \frac{T_ik^2}{2\rho_iA_i} + \frac{k\sigma_{1,i}}{2} + \frac{k}{2}\sqrt{\left(\frac{T_ik}{\rho_iA_i} + 4\sigma_{1,i}\right)^2 + \frac{16E_iI_i}{\rho_iA_i}}. \tag{57}$$

3.7. System update

In the implementation, the string displacement $\mathbf{u}_i^{n+1}$ is not updated directly using equation (32), since the gradient g_i^n (33, 34) requires the update of the system in the absence of the contact potential. Instead, $\mathbf{u}_i^{n+1}$ is updated by solving (37). Therefore, at each time step, the coupling force $f_{c,i}^n$ and the friction force $f_{b,i}^n$ are first obtained by solving (45) and (52). Subsequently, these forces are employed to update the states of the strings and the finger, denoted as $\mathbf{u}_1^*$, $\mathbf{u}_2^*$, and U_f^*, in the absence of finger-string contact forces:

$$\begin{aligned}\mathbf{u}_i^* =&A_{s,i}^{-1}\mathbf{B}_{s,i}\mathbf{u}_i^n + A_{s,i}^{-1}\mathbf{C}_{s,i}\mathbf{u}_i^{n-1} - A_{s,i}^{-1}\mathbf{J}_{b,i}^n f_{b,i}^n + A_{s,i}^{-1}\mathbf{J}_{c,i}^n f_{c,i}^n,\\ U_f^* =&2U^n - U^{n-1} + k^2 f_{\text{ext}}^n/M_f.\end{aligned} \tag{58}$$

With $\mathbf{u}_1^*$, $\mathbf{u}_2^*$, and U_f^*, the gradient g_i^n can be evaluated, after which $\mathbf{u}_i^{n+1}$ and U^{n+1} can be computed by (37). With obtained $f_{c,i}^n$, the modal displacements of the bridge are updated by:

$$\mathbf{q}^{n+1} = \text{diag}(\mathbf{A}_q)\mathbf{q}^n + \text{diag}(\mathbf{B}_q)\mathbf{q}^{n-1} - \text{diag}(\mathbf{C}_q)\left(\mathbf{f}_{c,1}^n + \mathbf{f}_{c,2}^n\right), \tag{59}$$

With obtained $f_{b,i}^n$, the bow hair displacement ζ^{n+1} is updated by,

$$\zeta_i^{n+1} = A_h\zeta_i^n + B_h\zeta_i^{n-1} - C_h f_{b,i}^n, \tag{60}$$

where $A_h = \left(8M_h - 2k^2K_h\right)/\lambda$, $B_h = (-4M_h - k^2K_h + 2kR_h)/\lambda$, $C_h = k^2/\lambda$, and $\lambda = 4M_h + k^2K_h + 2kR_h$. The average bristle deflection $\mu_{t\circ}z^n$ is simultaneously gained by iteratively solving (52), and it is used to update the next half-step bristle state via $z^{n+1/2} = 2\mu_{t\circ}z^n - z^{n-1/2}$.

4. PHYSICAL CHARACTERIZATION

4.1. String parameters

The strings of the yehu are traditional woven silk strings and their physical parameters were determined through a series of measurements. The string density was determined by measuring the mass and the volume of multiple string samples. The mass of each sample was measured using a high-precision balance. The volume of each sample was estimated by measuring the sample's radius and assuming a perfect cylindrical geometry. The Young's modulus, tension, and damping coefficients were identified via an inverse modeling procedure [19] from force signal measurements of a silk string excited via the wire-breaking method. To isolate the string from body resonances, the measurement was conducted on an anti-vibration optical table using custom 3D-printed sensor bridges. These measurements form the basis for the parameterization of the string model used in the subsequent simulations and these parameters are listed in Table 1.

4.2. Bridge admittance

The bridge admittance was obtained by exciting the bridge using an impact hammer (PCB Model 086C01), and capturing the resulting bridge velocity response with a Laser Doppler vibrometer (LDV) (Polytec PDV-100). The blue curve in the upper panel of Fig. 2 displays the bridge admittance, while the blue curve in the lower panel displays the bridge velocity in response to the hammer impact. The admittance was processed using the filter diagonalization method [20] to extract the modal parameters. The identified modal parameters were then used to derive the body modes, as formulated in (41). For comparison, the MSD system with 11 modes was excited using the measured hammer force, and the resulting simulated responses are depicted by the red dashed curves in Fig. 2.

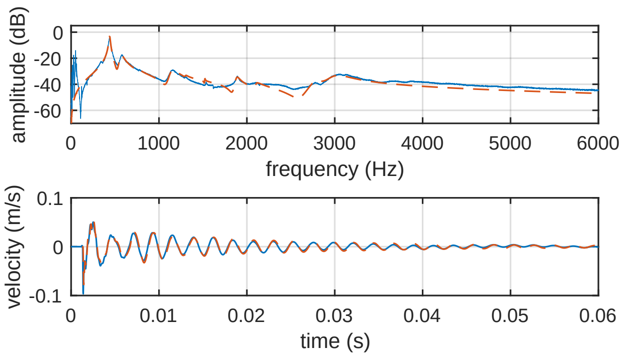

Figure 2: Measured (blue) and simulated (red, dashed) bridge admittance (top) and velocity (bottom).

4.3. Body radiation filter

The transfer function from bridge force to radiated sound pressure was obtained from impact hammer measurements conducted in a hemi-anechoic chamber with a pair of microphones (HBK Type 4190) placed 30 cm behind the soundbox. The transfer function was approximated using a parallel infinite impulse response (IIR) filter structure, which, compared to direct-form IIR implementations, generally exhibits improved numerical performance [21]. The radiation filter was designed by fitting 25 sections to the measured transfer function in the warped frequency domain. The fitted response is in good agreement with the measured data over the relevant frequency range, indicating a reasonable approximation. The radiated sound is then synthesized by filtering the simulated bridge force.

5. SIMULATION RESULTS

5.1. String-bridge coupling

As shown in Fig. 2, the model provides a good fit to the bridge velocity when excited by a measured impact force. The total behavior of the system is validated by comparing measured and simulated bridge velocities while the instrument is being bowed. A measurement was conducted by fixing the yehu and manually bowing the F4 string while capturing the bridge velocity using an LDV.

Table 1: Measured and derived silk string parameters.

	String 1 (F4)	String 2 (C5)	
L	0.38	0.38	m
ρ	1250	1350	kg/m^3
r	0.55	0.40	mm
T	50.61	64.29	N
E	1×10^{10}	9.5×10^9	Pa
σ_0	0.9754	1.5844	s^{-1}
σ_1	0.0026	0.0032	m^2/s

Figure 3 compares the measured and simulated steady-state bridge velocity in the time domain. Since no apparatus was available to precisely control or measure the bow force and velocity during the experiment, their values in the measurement remain unknown. Nevertheless, a close agreement in Fig. 3 was obtained by tuning the simulated bow force and bow velocity parameters. In particular, a good fit was obtained when the bow force and bow velocity were set to constant values of 0.7 N and 0.3 m/s, respectively. It was also observed that increasing the bow velocity slightly above 0.3 m/s leads to a simulated bridge velocity with a larger amplitude, whereas decreasing the bow velocity results in a smaller amplitude.

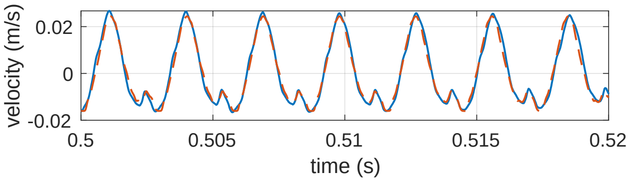

Figure 3: Measured (blue) and simulated (dashed, red) bowed bridge velocity on string 1 (tuned to F4)

5.2. Finger-string interaction

In the proposed model, the finger-string contact is modeled as a collision. The corresponding parameters, finger stiffness K_f, nonlinear coefficient α, and damping coefficient β, are not obtained from direct measurements. Instead, they are selected empirically based on simulation outcomes to yield physically plausible behavior. In the following simulations, the parameters are set as $K_f = 5 \times 10^5$, $\alpha = 2.3$, and $\beta = 20$. Fig. 4 illustrates the simulated transverse displacement of the two coupled strings at four representative time instants under bowed excitation and finger pressing. The bow is driven by a constant bow force of 0.7 N and a constant bow velocity of 0.3 m/s. The finger is driven by an external force of 0.5 N.

Figure 5 presents the spectrograms of two gestures, obtained from signals generated by filtering the simulated bridge force through a parallel IIR filter fitted to the radiation transfer function. In the upper spectrogram, two sinusoidal signals are used to modulate the bow force F_N and bow velocity v_b, enabling rapid alternation between two strings, as well as frequent bow direction changes. At $t = 1$ s, the finger, driven by an external force, comes into contact with the string, thereby playing new notes, while the bowing motion continues uninterrupted. In the lower spectrogram, string 1 is bowed without bow direction changes, while the finger presses both strings with slight oscillatory motion along the strings. Finger glides at $t = 0.5s$ and $1s$ yield higher pitches. Sound samples and simulation codes are available on the companion website. [1]

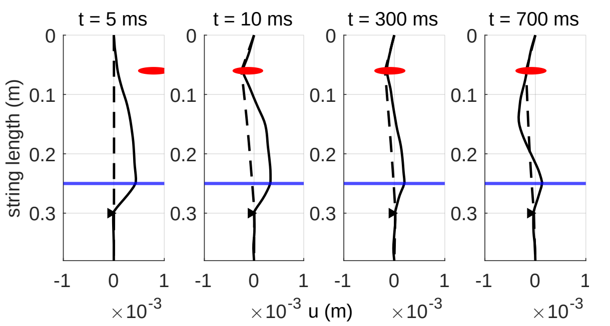

Figure 4: String transverse displacement profiles at selected time instants. The red ellipse denotes the finger, the blue line denotes the bow, the black solid line represents string 1, the black dashed line represents string 2, and the triangle indicates the bridge. The overlapping of the solid and dashed black lines with the red ellipse illustrates the finger-strings penetration η_i.

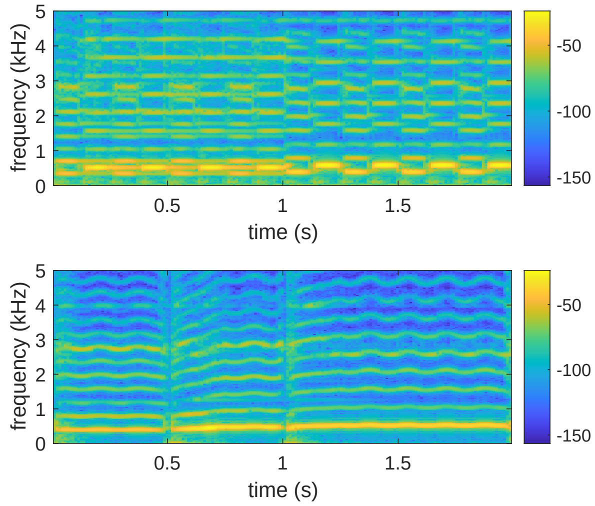

Figure 5: Spectrograms of two gestures. Gesture 1: rapid changes in bowing direction and bowing string, with the finger pressing both strings simultaneously at $t = 1s$. Gesture 2: vibrato produced by slight finger motion during pressing, with finger glides at $t = 0.5s$ and $t = 1s$, resulting in higher pitches.

5.3. System energy evolution

Fig. 6 presents the time evolution of the system energy error, with random finger pressing position and continuous bowing, where the system energy error is calculated by $\mathfrak{e}^n = \delta_{t-}\mathfrak{h}^{n+\frac{1}{2}} - \mathfrak{p}^n + \mathfrak{q}^n - \mathfrak{b}^n$. The results show that the energy deviation remains on the order 10^{-15} throughout the 10-second simulation, indicating that the numerical scheme preserves energy with near machine-precision accuracy.

5.4. Real-time factor

The proposed numerical scheme was implemented in C++. It was found, through experimentation, that the number of iterations required to update the bow force is inversely dependent on the magnitude of the force f_N. By limiting the minimum absolute force to 0.05 N, the maximum number of required iterations was only three at a sampling rate of 44.1 kHz. On average, a 10 second sample required 1.49 seconds of computation time, while 20 second and 30 second inputs required 2.95 seconds and 4.5 seconds, respectively. This corresponds to a real-time factor of approximately 6.6× faster

[1]Companion website with sound samples and simulation codes: https://yehudafx26.github.io/

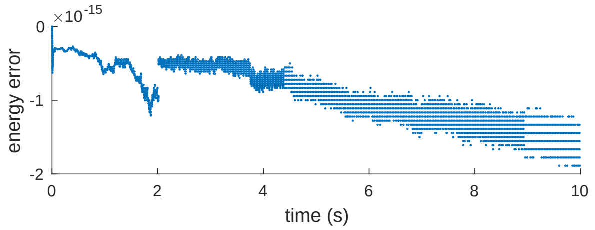

Figure 6: Energy error with time evolution.

than real-time. The simulations were run on a 2020 MacBook Pro equipped with an Apple M1 chip.

6. CONCLUSIONS AND FUTURE WORK

In conclusion, this paper proposes a physical model of the yehu, implemented using a FD scheme with measurement-based physical characterization. The simulation results demonstrate that the string-bridge coupling strategy is capable of fitting the measured bridge motion under bow-string excitation. The inclusion of finger-strings interactions and real-time performance further enhance the playability of the model, supporting future implementation in real-time interactive sound synthesis applications. Future work will focus on both model refinements and playability analysis. The model can be extended by incorporating multiple fingers, as yehu performers may use up to four fingers, and by accounting for multi-dimensional finger–string contact interactions. In addition, vibrato in yehu performance may arise from fluctuations in string tension induced by variations in finger pressing force; thus, a tension-modulated string model will be considered. Finally, further investigation of parameter design and gesture control will be undertaken to evaluate and enhance the playability of the numerical model.

7. ACKNOWLEDGMENTS

Zhen Zheng gratefully acknowledges the financial support provided by the China Scholarship Council. The authors would like to thank Alexander Mayer for providing circuit schematics and designs for the string measurement system; Jianyu Li for access to the Young's modulus apparatus; and Luc Mongeau for providing the high-precision balance. The authors also thank the anonymous reviewers for their valuable comments.

8. REFERENCES

[1] J. H. Smith and J. Woodhouse, "The tribology of rosin," *J. Mech. Phys. Solids*, vol. 48, no. 8, pp. 1633–1681, 2000.

[2] P. M. Galluzzo, "On the playability of stringed instruments," Ph.D. dissertation, University of Cambridge, 2004.

[3] P. Dupont, B. Armstrong, and V. Hayward, "Elasto-plastic friction model: contact compliance and stiction," in *Proc. Amer. Control Conf.*, vol. 2. IEEE, 2000, pp. 1072–1077.

[4] J. Woodhouse, "Bowed string simulation using a thermal friction model," *Acta Acustica united with Acustica*, vol. 89, pp. 355–368, 2003.

[5] S. Serafin, F. Avanzini, D. Rocchesso *et al.*, "Bowed string simulation using an elasto-plastic friction model," in *Proc. Stockholm Music Acoustics Conf., 2003*. Royal Institute of Technology, 2003, pp. 95–98.

[6] E. Maestre, C. Spa, and J. O. Smith III, "A bowed string physical model including finite-width thermal friction and hair dynamics," in *Proc. Int. Computer Music Conf.*, 2014.

[7] C. G. M. Desvages, "Physical modelling of the bowed string and applications to sound synthesis," Ph.D. thesis, University of Edinburgh, Edinburgh, UK, 2018.

[8] E. Matusiak, V. Chatziioannou, and M. van Walstijn, "A refined bow-string interaction model considering hysteresis," in *Proc. Mtgs. Acoust.*, vol. 58, no. 1. Acoustical Society of America, 2025, p. 035014.

[9] E. Matusiak, V. Chatziioannou, and M. van Walstijn, "Numerical modelling of elasto-plastic friction in bow string interaction with guaranteed passivity," *Front. Signal Process*, vol. 5, p. 1525044, 2025.

[10] H. Mansour, J. Woodhouse, and G. Scavone, "On minimum bow force for bowed strings," *Acta Acustica united with Acustica*, vol. 103, pp. 317–330, 2017.

[11] O. Inácio, J. Antunes, and M. Wright, "Computational modelling of string–body interaction for the violin family and simulation of wolf notes," *J. Sound Vib.*, vol. 310, no. 1-2, pp. 260–286, 2008.

[12] S. Bilbao, R. Russo, C. Webb, and M. Ducceschi, "Real-time guitar synthesis," in *Proceedings of the 27th International Conference on Digital Audio Effects ((DAFx24)*, 2024, pp. 163–170.

[13] V. Chatziioannou and M. van Walstijn, "Energy conserving schemes for the simulation of musical instrument contact dynamics," *J. Sound Vib.*, vol. 339, pp. 262–279, 2015.

[14] S. Bilbao, A. Torin, and V. Chatziioannou, "Numerical modeling of collisions in musical instruments," *Acta Acustica united with Acustica*, vol. 101, 05 2014.

[15] M. van Walstijn, V. Chatziioannou, and A. Bhanuprakash, "Implicit and explicit schemes for energy-stable simulation of string vibrations with collisions: Refinement, analysis, and comparison," *J. Sound Vib.*, vol. 569, p. 117968, 2024.

[16] M. Ducceschi and S. Bilbao, "Non-iterative solvers for non-linear problems: the case of collisions," in *Proc. Intl. Conf. Digital Audio Effects (DAFx19)*, 2019.

[17] S. Bilbao, *Numerical Sound Synthesis Finite Difference Schemes and Simulation in Musical Acoustics*. John Wiley and Sons, Ltd., 2009.

[18] J. Sherman and W. J. Morrison, "Adjustment of an inverse matrix corresponding to a change in one element of a given matrix," *The Annals of Mathematical Statistics*, vol. 21, no. 1, pp. 124–127, 1950.

[19] A. Lampis, A. Mayer, and V. Chatziioannou, "An experimental approach for comparing the influence of cello string type on bowed attack response," *JASA Express Lett.*, vol. 4, p. 113201, 2024.

[20] E. Ó. Néill, M. Ortiz, and M. van Walstijn, "Tunable instrument body resonances: from measured instrument body impulse response to parameteric convolution," in *Proc. Int. Comp. Music. Conf.*, 2022, pp. 89–92.

[21] B. Bank, "Converting infinite impulse response filters to parallel form [tips & tricks]," *IEEE Signal Process. Mag.*, vol. 35, no. 3, pp. 124–130, 2018.